18th European Conference on Earthquake Engineering

Accounting for damage accumulation in seismic fragility functions via hysteretic energy

Serkan Hasanoglu[1], Gerard J. O'Reilly[1]

1- Centre for Training and Research on Reduction of Seismic Risk (ROSE Centre), Scuola Universitaria Superiore IUSS di Pavia, Pavia 27100, Italy

serkan.hasanoglu@iusspavia.it

Abstract

Accurate quantification of cumulative damage remains a significant challenge for seismic risk studies, particularly for regions affected by long-duration ground motions or earthquake aftershock sequences. Typically, seismic fragility studies rely on peak response quantities, such as displacement or drift, which fail to capture the accumulation of structural damage under cyclic loading. To overcome this limitation, this study presents a hysteretic energy-based methodology for seismic fragility assessment of reinforced concrete (RC) frame buildings based on experimentally calibrated cyclic backbone and hysteretic energy capacity, $E_{\mathrm{h,cap}}$, models. To this end, a database of reversed cyclic column tests was first compiled and filtered to obtain a representative subset of experiments for typical RC buildings, and was later used for model calibrations. Based on the proposed $E_{\mathrm{h,cap}}$ formulation, an energy-based damage index was developed to consistently quantify the progression of flexural damage in RC building structures. The models for the calibrated cyclic backbone parameters, $\mathrm{E_{h,cap}}$, and the proposed damage index were then implemented in a three-dimensional numerical model, and time-history analyses were conducted to compare the effects of each structural assessment method. The results demonstrate that the proposed methodology improves the representation of cyclic behaviour, and the difference between the two approaches becomes critical, particularly at high levels of structural damage.

Keywords: Energy-based structural assessment, nonlinear analysis, structural vulnerability, hysteretic energy capacity.

1- INTRODUCTION

Assessing seismic risk and potential losses for building portfolios is essential for developing effective risk mitigation strategies in earthquake-prone regions. A typical regional seismic risk assessment study combines three main components: a probabilistic seismic hazard model, an exposure dataset describing the building stock, and vulnerability functions that represent the relationship between ground-motion intensity and expected damage or losses. Various approaches have been proposed in the literature for deriving fragility or vulnerability functions with different levels of complexity [1, 2], and the choice of method generally depends on the availability of building data and the desired balance between computational efficiency and modelling accuracy.

Numerical models used in such analyses can vary in their level of structural idealisation. Equivalent single-degree-of-freedom (SDOF) models [3, 4] are commonly employed due to their simplicity and computational efficiency, while two-dimensional multi-degree-of-freedom (MDOF) models [5, 6] provide improved representation of structural behaviour at moderate computational cost. Three-dimensional (3D) detailed MDOF models provide the most representative structural behaviour, though at a higher computational cost. However, advances in computational resources have enabled the increasing use of 3D MDOF models for regional-scale simulations [7, 8]. Furthermore, several frameworks have been developed to facilitate the systematic generation of large building portfolios of 3D models [9, 10].

Among these, 3D models adopt either fibre-based models or phenomenological hinge models at the element level. Fibre-based formulations [11, 12] represent material non-linearity through constitutive laws [13, 14] and can capture axial force–bending moment interaction and biaxial bending effects directly. However, their high computational cost and difficulty in representing cyclic deterioration mechanisms limit their practicality in large-scale simulations. On the other hand, phenomenological hinge models [15–18] offer a computationally efficient alternative by representing inelastic behaviour through moment-rotation relationships assigned at plastic hinge locations.

Apart from modelling, structural damage is typically assessed using displacement-based engineering demand parameters (EDPs), such as the peak storey drift (PSD). While these measures are practical, they overlook cumulative damage effects that could be significant, especially during long-duration ground motions or earthquake sequences. On the other hand, the assessment of building structures, particularly those designed in accordance with modern seismic design codes, should not rely solely on displacement-based criteria. Due to their high ductility, such structures can withstand large displacements without collapsing. Additionally, the drift-based damage state thresholds used to generate fragility models are often questionable for these structures. As an alternative to displacement-based EDPs, energy-based damage indices offer a better representation of cyclic damage. However, none of these definitions included the hysteretic energy capacity, $E_{h,cap}$, of structural elements, a physically meaningful metric for assessing the level of flexural damage, in these formulations. Nevertheless, accurately quantifying $E_{h,cap}$ is difficult due to the complex interaction between loading history and material behaviour [19].

To address these issues, this study first introduces empirical models calibrated for the four-segment cyclic backbone curve parameters of ductile RC beam-column elements, using filtered experimental data that represent the properties of typical RC building structures. Subsequently, an empirical model for estimating the $E_{h,cap}$ of flexure-dominated RC beam–column elements is proposed. Based on this, a novel $E_{h,cap}$-based damage index is developed. Moreover, the cyclic degradation parameters of the *HystereticSM* material model in *OpenSees* [20], which is used to model the four-segment backbone for this study, are examined to facilitate consistent tracking of hysteretic behaviour under cyclic loading. Later, the proposed models are tested in an example application that compares the analysis results attained using displacement-based and energy-based procedures.

2- MODEL CALIBRATIONS

2-1- SELECTION OF EXPERIMENTAL DATA

The experimental dataset used for model calibration was derived from the recently refined version of the ACI 369 Rectangular Column Database [21]. The updated database contains 234 reversed-cyclic pushover tests of rectangular RC columns. In addition, 10 experiments from the literature [22, 23] were included, bringing the total to 244 tests. The database provides force-displacement histories, geometric properties, material characteristics, and failure modes for each specimen. Because the full dataset includes a wide range of mechanical properties and failure mechanisms that are not always representative of typical ductile RC frame columns, a two-stage filtering process was applied. First, only specimens exhibiting flexure-dominated damage behaviour were retained, while those governed by shear or combined flexure–shear failure modes were excluded. Second, an additional filtering was performed based on the experimental mechanical properties. Specifically, specimens were required to satisfy limits on axial load ratio ($\nu \leq 0.7$), concrete compressive strength ($f_c < 80$ MPa), steel yield strength of longitudinal and transverse reinforcements (f_{yl} and $f_{yt} < 600$ MPa), longitudinal reinforcement ratio ($\rho_l \leq 0.04$), and shear span length to effective depth ratio ($L_s/d \geq 2$). After applying these criteria and removing some low-quality tests, 97 experiments remained. To expand the dataset, 18 additional experiments that met these criteria but were excluded from the original ACI database due to lack of access to original studies were included, resulting in a final dataset of 115 tests for model calibration.

2-2- CALIBRATIONS FOR CYCLIC BACKBONE CURVE PARAMETERS

After compiling the experimental dataset, this section presents predictive equations for six model parameters that define the four-segment cyclic backbone curve as illustrated in Figure 1. These parameters include:

- The ratio of the secant stiffness at the yield point to the gross section stiffness, EI_y/EI_g, to determine the yield rotation, $\theta_y = M_yL_s/(3EI_y)$, where L_s is the shear span length, which can be assumed as the half-length of structural elements.
- The plastic rotation before the capping point, θ_{pl}.
- The post-capping plastic rotation between the capping and ultimate point, θ_{pc}.
- The post-ultimate rotation between the ultimate and the zero-moment point, θ_{pu}.
- The moment ratio representing strain hardening, M_{cap}/M_y.
- The moment ratio representing strain softening, M_{ult}/M_{cap}.

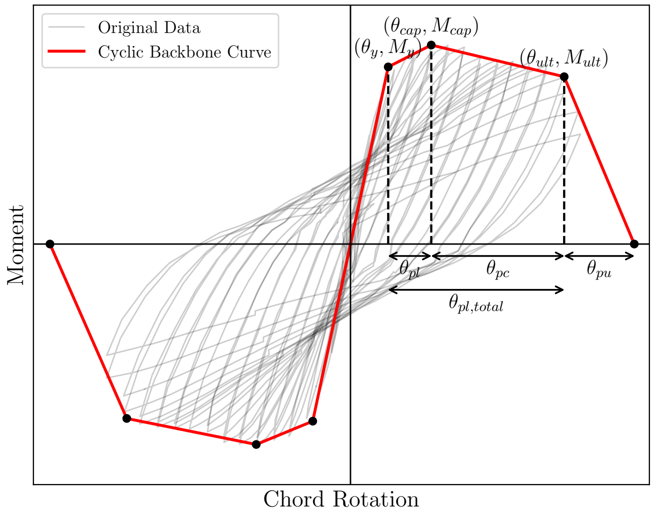

Figure 1- The parameters defining the cyclic backbone curve.

The calibration process starts with analysing how model parameters relate to key predictor variables. The form of each equation was identified through an iterative process. Initially, an equation was selected based on observed trends, then refined by retaining only predictor variables that are statistically significant at the 95% confidence level, as determined by the standard F-test. Non-linear least-squares regression was used to calibrate the coefficients in the multiplicative form, consistent with previous research [15, 16]. The calibration was based on the natural logarithms of the parameters, assuming a lognormal distribution. Ultimately, the equations provide median estimates of the parameters, with prediction uncertainty quantified by the logarithmic standard deviation, σ_{LN}. The calibrated equations for the cyclic backbone parameters are given in Equations 1 to 6, where ν is the axial load ratio, L_s/d is the shear span length to effective depth ratio, f_c' and f_{yl} are concrete compressive strength and steel yield strength of longitudinal steel reinforcements, ρ_l is the longitudinal reinforcement ratio, and ρ_t is the transverse reinforcement ratio.

$$\frac{EI_y}{EI_g} = 0.08 \times 1.25^{10\nu} \times 1.2^{L_s/d}, 0.2 \leq \frac{EI_y}{EI_g} \leq 0.8, \ \sigma_{LN} = 0.24 \quad (1)$$

$$\theta_{pl} = 0.009 \times 0.25^{0.01f_c'} \times 0.23^{\nu} \times 2.17^{100\rho_l}, \ \sigma_{LN} = 0.56 \quad (2)$$

$$\theta_{pc} = 0.01 \times 0.07^{\nu} \times 1.78^{100\rho_t} \times 1.18^{0.01f_{yl}}, \ \sigma_{LN} = 0.44 \quad (3)$$

$$\theta_{pu} = 0.0023 \times 1.96^{0.1f_c'} \times 2.74^{100\rho_t}, \text{where } \theta_{pu} \leq 4\theta_{pc}, \ \sigma_{\mathrm{LN}} = 0.22 \quad (4)$$

$$\frac{M_{cap}}{M_y} = 1.08^{\nu} \times 1.38^{10\rho_l} \times 1.14^{0.1L_s/d}, \ \sigma_{LN} = 0.04 \quad (5)$$

$$\frac{M_{ult}}{M_{cap}} = 0.91^{0.01f_c'} \times 0.80^{0.1L_s/d}, \ \sigma_{LN} = 0.07 \quad (6)$$

For the yielding moment, the equation proposed by Panagiotakos and Fardis [16] showed good agreement with experimental values; therefore, this formula was used in this study. The four-point cyclic backbone curve is modelled using the *HystereticSM* material model in *OpenSees*, which supports multipoint backbone definitions. An additional calibration study was conducted to optimise the cyclic degradation parameters of *HystereticSM*, minimising the difference between experimental data and numerical results. Ultimately, the parameter sets (*pinchx*=1.0, *pinchy*=1.0, *damage1*=0, *damage2*=0.2 *and beta*=0.4) and (*pinchx*=0.5, *pinchy*=0.5, *damage1*=0, *damage2*=0.7, *beta*=0.2) are recommended for columns and beams respectively.

2-3- EMPIRICAL MODEL FOR THE HYSTERETIC ENERGY CAPACITY OF RC BEAM-COLUMN ELEMENTS

Following the development of predictive equations for the cyclic backbone parameters, this sub-section presents the empirical model given in Equation 7 for the $E_{h,cap}$ of RC beam–column sections. This formula is expressed in terms of three key parameters: the yield moment, M_y, the total plastic rotation capacity, $\theta_{pl,total} = \theta_{pl} + \theta_{pc}$, and the λ parameter. Here, λ is defined as the ratio of the $E_{h,cap}$ to the product of M_y and $\theta_{pl,total}$, and the empirical equation in Equation 8 is thus proposed as:

$$E_{h,cap} = M_y \times \theta_{pl,total} \times \lambda \tag{7}$$

$$\lambda = 52 \times 0.41^{0.01(f_c' + 0.1 f_{yl})} \times 0.34^{\nu} \times 0.21^{s_t/h}, \sigma_{LN} = 0.30 \tag{8}$$

where s_t is the transverse reinforcement spacing within the confinement zone, and h is the section depth. Figure 2 compares the observed values of λ and $E_{h,cap}$ with predictions from both the proposed equations and those in the literature. The comparison shows that the predictions of λ and $E_{h,cap}$ from the proposed equations align well with experimental results. Additionally, two formulations proposed by Haselton et al. [15] (one based on λ and the other on γ, following their notation) are used to compare the predicted $E_{h,cap}$ values. As illustrated in the figure on the right, the first formula overestimates $E_{h,cap}$, and both of them exhibit greater dispersion than the proposed equation, likely due to differences in the experimental datasets used for model calibration.

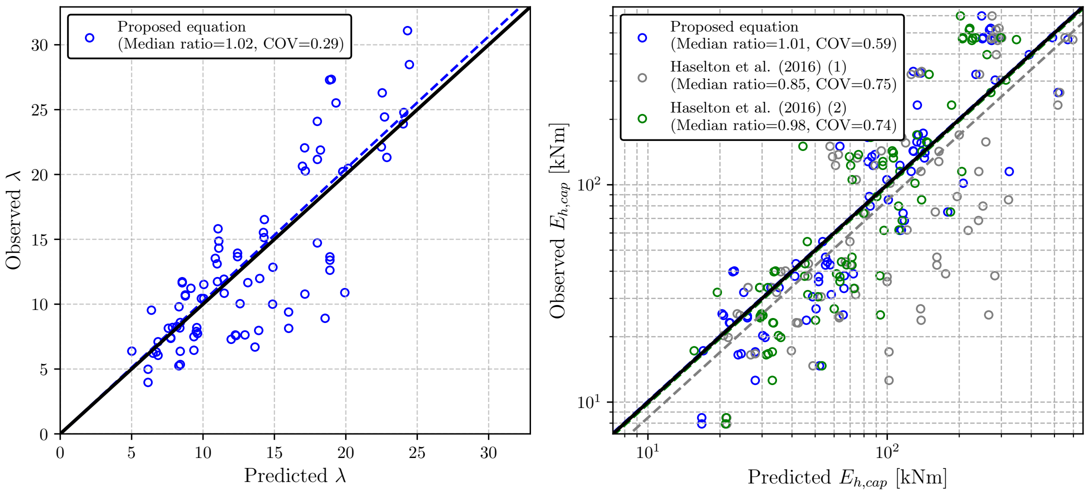

Figure 2- Comparison of observed values of λ and $E_{h,cap}$ with predicted values from the proposed and literature equations.

3- HYSTERETIC ENERGY-BASED DAMAGE INDEX

Once the empirical equation for the $E_{h,cap}$ is calibrated, both local (at hinge level) and global (at structure level) energy-based damage indices can be defined for a particular 3D RC frame structure. For structural members experiencing uni-directional bending (e.g., beams), the damage index (DI) for plastic hinge i is given by Equation 9, as the ratio of the total hysteretic energy dissipated during cyclic loading to the corresponding $E_{h,cap}$ where the dissipated hysteretic energy represents the enclosed area under the moment–rotation hysteresis loops, with the moment and rotation quantities obtainable via the "*eleResponse*" method or element recorders in *OpenSees*. An additional criterion is used here: if the rotation demand during cyclic loading exceeds θ_{ult}, the limit rotation value in the cyclic backbone curve, the DI is assigned a value of 1, which represents the loss of that specific member's load-carrying capacity. This criterion ensures physical consistency with the member's cyclic backbone behaviour. The DI is also capped at 1 to prevent artificially inflating the structure-level DI in Equation 11.

For column hinges subjected to bi-directional bending, simultaneous damage in two perpendicular directions has a combined effect on the overall damage of the hinge. Therefore, the interaction between these two directions should be considered. Additionally, note that the cyclic backbone behaviour for each column-hinge direction is assumed to be independent under loading, a common approach in the literature when modelling column hinges with the concentrated plasticity approach. This assumption does not fully capture the real physical behaviour, because damage in one direction of loading can also affect the response in the other direction due to the shared material state.

Following this modelling assumption, DI values are initially calculated for the two orthogonal loading directions at each column hinge independently using Equation 9. Afterwards, the overall DI of the column hinge is determined using the square root of the sum of squares (SRSS) method as in Equation 10, where $DI_{i,x}$ and $DI_{i,y}$ denote the damage values in the two principal axes of bending of the member, denoted x and y, to indirectly consider the interaction of the two directions. This assumption was also verified using experimental data from biaxially loaded column tests in Rodrigues et al. [22], based on the DI definition adopted herein. Similar to beams, the DI of column hinges is capped at 1.

$$DI_{uni-direct,i} = \begin{cases} 1, \; \theta_i > \theta_{ult} \\ min\left(1, \frac{\sum E_{h,i}}{E_{h,cap}}\right), \; otherwise \end{cases} \tag{9}$$

$$DI_{bi-direct,i} = min\left(1, \sqrt{DI_{i,x}^2 + DI_{i,y}^2}\right) \tag{10}$$

Once the local damage indices are determined using Equations 9 and 10, the DI for storey j can be determined as the energy-weighted average of the damage indices within that storey, as given with Equation 11. In this formula, DI_{ji} represents the damage index at hinge i of storey j, E_{ji} is the total hysteretic energy dissipated by that hinge during cyclic loading, m denotes the total number of hinges within that storey (including both beam and column hinges) and $E_{j,total}$ is the total hysteretic energy dissipated at storey j during cyclic loading.

$$DI_j = \frac{\sum_{i=1}^{m} DI_{ji} E_{ji}}{E_{j,total}} \tag{11}$$

To account for the influence of the failure mechanism on the overall damage state of the structure, Equation 11 is applied separately to the column and beam hinges within each storey j, yielding $DI_{j,col}$ and $DI_{j,beam}$, respectively. A mechanism index η_j is then defined as in Equation 12, where η_j ranges between 0 and 1. A value of $\eta_j \approx 0$ indicates a beam-sway mechanism where damage is concentrated in beam hinges, which is the desired behaviour under seismic loading. Conversely, $\eta_j \approx 1$ indicates a column-sway mechanism associated with soft-storey behaviour, which is significantly more detrimental to structural safety. The overall DI of the structure is then defined as in Equation 13, which penalises storeys exhibiting column-sway behaviour through the mechanism-weighted term $(1 + \eta_j)$, which is bounded between 1.0 and 2.0 by definition. A pure beam-sway mechanism leaves the storey DI unchanged, while a pure column-sway mechanism doubles its contribution to the overall DI. This amplification reflects the greater damage caused by column-sway mechanisms, which are associated with soft-storey behaviour and a significantly higher risk of collapse than beam-sway mechanisms, where damage is more uniformly distributed across the structure.

$$\eta_j = \frac{DI_{j,col}}{DI_{j,col} + DI_{j,beam}} \tag{12}$$

$$DI_{struct} = \max\left(DI_j (1 + \eta_j)\right) \tag{13}$$

To establish the DI thresholds for different damage states, experiments from the filtered experimental dataset, which contain displacement values associated with specific damage observations, are used. This subset includes data on concrete crushing (41 experiments), significant concrete cover spalling (30 tests), longitudinal bar buckling (32 experiments), longitudinal bar fracture (8 experiments), and loss of axial load capacity (6 experiments). For these cases, collapse is defined as occurring either through longitudinal bar fracture or loss of axial load capacity. Since some experiments reported bar fracture while some noted axial failure alone, both are considered equivalent, resulting in 13 total collapse observations within the subset.

For each experiment, the hysteretic energy dissipated up to the displacement corresponding to a specific damage level was computed and normalised by the total hysteretic energy dissipated up to the collapse case, $E_{h,cap}$. This procedure allowed the derivation of DI values for each physical damage state, and the resulting DI distributions are illustrated in Figure 3, ranging from concrete crushing (DS1) to collapse (DS4). Based on the statistical metrics of these distributions and the capping procedure applied in Equations 9 and 10, the proposed global DI thresholds are given in Table 1.

Table 1- Proposed ranges of the global energy-based damage index of four flexural damage states.

Damage State	Description of damage	Median	16th–84th percentiles	Proposed thresholds
Slight (DS1)	Concrete crushing	0.05	0.03–0.10	0.01–0.10
Moderate (DS2)	Significant concrete spalling	0.19	0.09–0.34	0.10–0.40
Extensive (DS3)	Longitudinal bar buckling	0.68	0.43–0.87	0.40–0.70
Collapse (DS4)	Longitudinal bar fracture & loss of axial load capacity	1.00	0.92–1.00	≥ 0.70

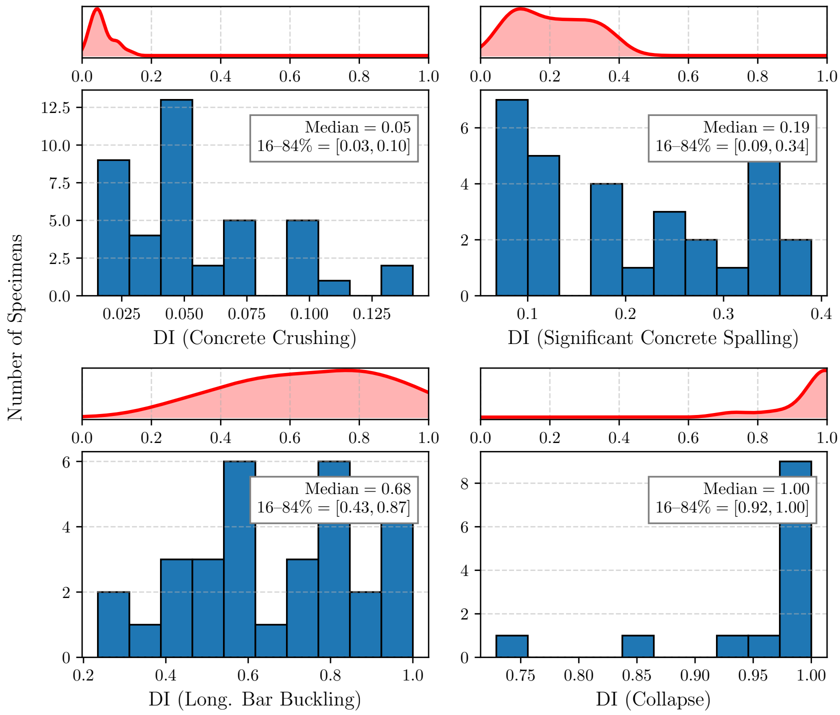

Figure 3- Calculated DI values corresponding to each defined damage state level in the experimental subset.

4- EXAMPLE APPLICATION

A four-storey RC frame building model was generated using the Simulated Design framework [10] for an example application, with structural properties summarised in Table 2. The storey height was set as 3 m, and bay widths were taken as 5 m in the X-direction and 4 m in the Y-direction. The structural system includes a two-way solid slab 15 cm thick. A seismic design load coefficient $\beta = 0.1$ was used to specify the lateral seismic load. The building was designed using C25 concrete and S420 reinforcing steel.

Additionally, all columns were assumed to have square cross-sections, and beams were modelled as emergent-type beams. The seismic design procedure followed the properties in the *tr_0018_dch* design class, which is one of the design classes [9] recently integrated into the framework for Turkish RC frame buildings. This class follows the provisions of the 1998 Turkish Seismic Design Code and TS500 RC design standard, by ensuring high-ductility requirements and employing the strong-column/weak-beam philosophy.

Table 2- General structural properties of the example RC frame building model.

Number of storey:	4	Design class:	tr_0018_dch
Storey height:	3m	Beta:	0.1
Number of bays in X direction:	4	Concrete grade:	C25
Number of bays in Y direction:	4	Steel grade:	S420
Bay width in X direction:	5 m	Column section:	square
Bay width in Y direction:	4 m	Beam section:	emergent
Slab type:	two-way solid slab	Slab thickness:	15 cm

After obtaining the design outputs, these parameters were used to generate the 3D non-linear model of the prototype structure using the concentrated plasticity approach in SimDesign. All beam-column elements were modelled with the *forcebeamcolumn* element in *OpenSees*, along with the *ConcentratedPlasticity* beam integration command, which assigns one plastic-rotation integration point at the ends of the element and three elastic-curvature integration points along its length [24]. For the plastic hinge properties, the equations calibrated in Section 2 were utilised. Meanwhile, beam-column joints were modelled as rigid, as joint failure is not anticipated in this building because of the design constraints specified in the aforementioned design codes. Infill walls at the perimeter of the building were modelled with low-quality infill properties, accounting for the effects of openings of infills, following the modelling procedure in the study of Hak et al. [25]. After creating the building model, modal analysis was performed, and the first mode vibration period of the structure was calculated to be approximately 0.38 s.

Later on, a probabilistic seismic hazard analysis (PSHA) was performed using the OpenQuake Engine [25] for a specific site in Istanbul, with a time-averaged shear-wave velocity in the uppermost 30 meters (V_{s30}) of 350 m/s. The ground-motion model for filtered incremental velocity at 0.38s period, FIV3(0.38), proposed by Aristeidou et al. [26] was employed. Seismic hazard disaggregation was also carried out for eight seismic-hazard levels, from an 80% probability of exceedance (POE) in 50 years to 0.5% POE in 50 years, and target spectrums that account for all significant causal earthquake scenarios for the study location for each hazard level were established for record selection, following the generalised conditional intensity measure approach [27]. In this process, FIV3(0.38s) was used as the conditioning IM, while FIV3(0.3), FIV3(0.5), FIV3(0.8) and $S_{a,avg2}(0.38)$ were used as the conditioned IMs. The correlation models from Aristeidou et al. [29] were employed, and the record selection process was carried out using the Djura ground-motion record selector [30].

After establishing the ground-motion set, a multiple-stripe analysis (MSA) was performed on the building model, and Figure 4 compares the resulting PSD and $E_{h,cap}$-based DI values. This comparison reveals several noteworthy trends. First, the scatter between PSD and DI increases progressively with intensity level, which is to be expected: at higher intensities, damage accumulates more extensively, and this accumulation is not fully captured by PSD alone. Second, several collapse cases identified through the DI definition are associated with PSD values as low as 4–5%, a level of drift that would not typically be regarded as indicative of collapse in a ductile structure when assessed through drift-based method. Third, among the noncollapse cases identified by the DI definition, a given PSD value (e.g., 4%) can correspond to moderate or extensive damage states, showing that PSD does not properly capture the structure's condition. Taken together, these observations carry direct implications for fragility assessment: $E_{h,cap}$-based DI would likely produce a fragility curve with a different median and/or dispersion than one derived from a PSD-based evaluation, and could yield meaningfully better estimates of structural damage.

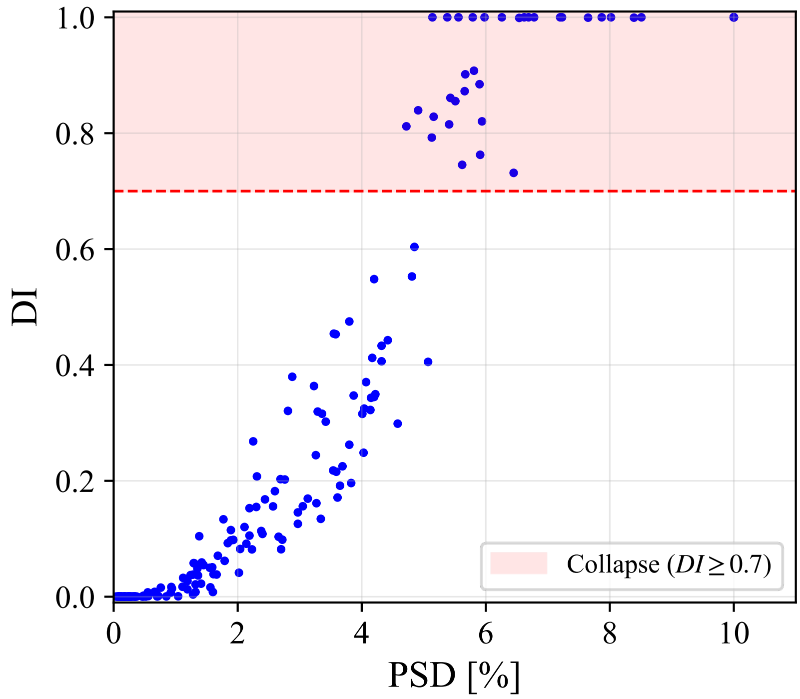

Figure 4- Comparison of PSD and $E_{h,cap}$-based DI values from MSA.

5- CONCLUSION

This study presented a hysteretic energy-based methodology for seismic fragility assessment of RC frame buildings, with a focus on accurately representing cumulative damage under cyclic loading. The following conclusions can be drawn:

- Predictive equations for the six parameters defining the four-segment cyclic backbone curve of ductile RC beam–column elements were calibrated against a filtered experimental dataset of 115 reversed-cyclic column tests. These equations provide median estimates of the backbone parameters along with associated prediction uncertainties.
- An empirical model for the hysteretic energy capacity, $E_{h,cap}$, of flexure-dominated RC beam–column elements was also proposed and calibrated using the same experimental dataset, demonstrating good agreement with experimental observations.
- Building on these models, a novel energy-based damage index (DI) was developed, which relies on the assumption of concentrated plasticity and incorporates $E_{h,cap}$ as a physically meaningful normalisation metric.
- The proposed DI accounts for uni-directional bending in beams and biaxial bending interaction in columns through an SRSS combination, and penalises column-sway mechanisms at the structure level through a mechanism-weighted formulation. This provides a more consistent representation of flexural damage progression than conventional displacement-based measures.
- A multiple-stripe analysis performed on an example four-storey ductile RC frame building showed that the scatter between PSD and the proposed DI increases progressively with intensity level, reflecting cumulative damage that PSD alone cannot capture. Several cases classified as collapse according to the DI definition were associated with PSD values as low as 4–5%, drift levels that conventional displacement-based methods would not typically identify as collapse; conversely, several noncollapse cases exhibited moderate-to-extensive damage at a given PSD value, indicating that displacement alone does not uniquely characterise the structure's damage state.

Overall, these findings indicate that a damage definition based on the proposed $E_{h,cap}$-based DI would likely yield fragility curves with a different median and/or dispersion than those obtained from a conventional PSD-based assessments, and can produce meaningfully better estimates of structural damage. This underscores the value of the proposed methodology for improving vulnerability assessment in scenarios where cumulative damage effects are critical.

6- ACKNOWLEDGMENT

Numerical simulations conducted in this paper have been performed on the High-Performance Computing DataCenter at IUSS, co-funded by Regione Lombardia through the funding programme established by Regional Decree No. 3776 of November 3, 2020. The ground motion record selections described here were performed using an academic licence of the Djura online ground motion record selector (www.djura.it).

7- REFERENCES

[1] Calvi, G.M.; Pinho, R.; Magenes, G.; Bommer, J.J.; Restrepo-Vélez, L.F.; Crowley, H.; Development of seismic vulnerability assessment methodologies over the past 30 years, ISET journal of Earthquake Technology, Volume 43, 2006, 75–104

[2] D'ayala, D.; Meslem, A.; Vamvatsikos, D.; Porter, K.; Rossetto, T.; Crowley, H.; Silva, V.; Guidelines for analytical vulnerability assessment of low/mid-rise buildings, GEM Technical Report, 2014

[3] Crowley, H.; Dabbeek, J.; Despotaki, V.; Rodrigues, D.; Martins, L.; Silva, V.; Romão, X.; Pereira, N.; Weatherill, G.; Danciu, L.; European seismic risk model (ESRM20), EFEHR Technical Report, Volume 2, 2021

[4] Erberik, M.A.; Fragility-based assessment of typical mid-rise and low-rise RC buildings in Turkey, Engineering Structures, Volume 30, 2008, 1360–1374

[5] Lu, X.; McKenna, F.; Cheng, Q.; Xu, Z.; Zeng, X.; Mahin, S.A.; An open-source framework for regional earthquake loss estimation using the city-scale nonlinear time history analysis, Earthquake Spectra, Volume 36, 2020, 806–831

[6] Ruggieri, S.; Chatzidaki, A.; Vamvatsikos, D.; Uva, G.; Reduced-order models for the seismic assessment of plan-irregular low-rise frame buildings, Earthquake Engineering and Structural Dynamics, Volume 51, 2022, 3327–3346

[7] Nafeh, A.M.B.; O'Reilly, G.J.; Fragility functions for non-ductile infilled reinforced concrete buildings using next-generation intensity measures based on analytical models and empirical data from past earthquakes, Bulletin of Earthquake Engineering, Volume 22, 2024, 4983–5021

[8] Zhang, W.; Chen, P.-Y.; Crempien, J.G.; Kurtulus, A.; Arduino, P.; Taciroglu, E.; Regional-scale seismic fragility, loss, and resilience assessment using physics-based simulated ground motions: an application to Istanbul, Earthquake Engineering and Structural Dynamics, Volume 52, 2023, 1785–1804

[9] Hasanoğlu, S.; Ozsarac, V.; O'Reilly, G.J.; A model for the simulated design of Turkish RC frame buildings in seismic vulnerability analysis, Bulletin of Earthquake Engineering, 2025, 1–28

[10] Ozsarac, V.; Pereira, N.; Mohamed, H.; Romão, X.; O'Reilly, G.J.; The Built Environment Data Framework for Simulated Design and Vulnerability Modelling in Earthquake Engineering, Earthquake Engineering and Structural Dynamics, 2025

[11] Spacone, E.; Filippou, F.C.; Taucer, F.F.; Fibre beam–column model for non-linear analysis of R/C frames: Part I. Formulation, Earthquake Engineering and Structural Dynamics, Volume 25, 1996, 711–725

[12] Spacone, E.; Filippou, F.C.; Taucer, F.F.; Fibre beam–column model for non-linear analysis of R/C frames: part II. Applications, Earthquake engineering and structural dynamics, Volume 25, 1996, 727–742

[13] Kent, D.C.; Park, R.; Flexural members with confined concrete, Journal of the structural division, Volume 97, 1971, 1969–1990

[14] Mander, J.B.; Priestley, M.J.; Park, R.; Theoretical stress-strain model for confined concrete, Journal of structural engineering, Volume 114, 1988, 1804–1826

[15] Haselton, C.B.; Liel, A.B.; Taylor-Lange, S.C.; Deierlein, G.G.; Calibration of model to simulate response of reinforced concrete beam-columns to collapse, ACI Structural Journal, Volume 113, 2016, 1141–1152

[16] Panagiotakos, T.B.; Fardis, M.N.; Deformations of reinforced concrete members at yielding and ultimate, Structural Journal, Volume 98, 2001, 135–148

[17] Elwood, K.J.; Shake table tests and analytical studies on the gravity load collapse of reinforced concrete frames, 2002

[18] Lignos, D.G.; Krawinkler, H.; Deterioration modeling of steel components in support of collapse prediction of steel moment frames under earthquake loading, Journal of Structural Engineering, Volume 137, 2011, 1291–1302

[19] Fardis, M.N.; From force-to displacement-based seismic design of concrete structures and beyond, European Conference on Earthquake Engineering Thessaloniki, Greece, 2018, 101–122

[20] Zhu, M.; McKenna, F.; Scott, M.H.; OpenSeesPy: Python library for the OpenSees finite element framework, SoftwareX, Volume 7, 2018, 6–11

[21] Avgin, S.; Koroglu, F.B.; Gullu, M.F.; Kose, M.M.; Refined Experimental Data Set for Reinforced Concrete Columns, Journal of Structural Engineering, Volume 152, 2026, 04725006

[22] Rodrigues, H.; Arede, A.; Varum, H.; Costa, A.; Damage evolution in reinforced concrete columns subjected to biaxial loading, Bulletin of earthquake Engineering, Volume 11, 2013, 1517–1540

[23] Kawashima, K.; Cyclic loading test data of reinforced concrete bridge piers, Effect of loading hysteresis on ductility capacity of reinforced concrete bridge piers. Journal of Structural Engineering, Volume 43, 1997, https://doi.org/10.60756/TITECH-VBTZ37H429

[24] Mazzoni, S.; Scott, M.H.; EFFICIENT CONCENTRATED-PLASTICITY MODELING IN OPENSEES

[25] Hak, S.; Morandi, P.; Magenes, G.; Sullivan, T.J.; Damage Control for Clay Masonry Infills in the Design of RC Frame Structures, Journal of Earthquake Engineering, Volume 16, 2012, 1–35, ISSN 1363-2469, 1559-808X, https://doi.org/10.1080/13632469.2012.670575

[26] Silva, V.; Crowley, H.; Pagani, M.; Monelli, D.; Pinho, R.; Development of the OpenQuake engine, the Global Earthquake Model's open-source software for seismic risk assessment, Natural Hazards, Volume 72, 2014, 1409–1427, ISSN 0921-030X, 1573-0840, https://doi.org/10.1007/s11069-013-0618-x

[27] Aristeidou, S.; Shahnazaryan, D.; O'Reilly, G.J.; Artificial neural network-based ground motion model for next-generation seismic intensity measures, Soil Dynamics and Earthquake Engineering, Volume 184, 2024, 108851, ISSN 02677261, https://doi.org/10.1016/j.soildyn.2024.108851

[28] Bradley, B.A.; A ground motion selection algorithm based on the generalized conditional intensity measure approach, Soil Dynamics and Earthquake Engineering, Volume 40, 2012, 48–61, ISSN 02677261, https://doi.org/10.1016/j.soildyn.2012.04.007

[29] Dávalos, H.; Miranda, E.; Filtered incremental velocity: A novel approach in intensity measures for seismic collapse estimation, Earthquake Engineering & Structural Dynamics, Volume 48, 2019, 1384–1405, ISSN 0098-8847, 1096-9845, https://doi.org/10.1002/eqe.3205

[30] Aristeidou, S.; Shahnazaryan, D.; O'Reilly, G.J.; Correlation models for next-generation amplitude and cumulative intensity measures using artificial neural networks, Earthquake Spectra, Volume 41, 2025, 851–875, ISSN 8755-2930, 1944-8201, https://doi.org/10.1177/87552930241270563

[31] Shahnazaryan, D.; Ozsarac, V.; O'Reilly, G.J.; DJURA GROUND MOTION RECORD SELECTOR: A SOFTWARE SOLUTION FOR EARTHQUAKE ENGINEERING, 2025, 740–757, https://doi.org/10.7712/120125.12444.25126